http://ansinet.com/itj

ITJ

ISSN 1812-5638

INFORMATION TECHNOLOGY JOURNAL

ANSInet
Asian Network for Scientific Information
308 Lasani Town, Sargodha Road, Faisalabad - Pakistan

Information Technology Journal 12 (14): 3042-3045, 2013
ISSN 1812-5638 / DOI: 10.3923/itj.2013.3042.3045

Study on the Aerodynamic Performance of Blade Airfoil of Vertical Axis Wind Turbine at Low Reynolds Number

[1]Zhao Li-Hua, [1]Liu Ming and [2]Lv Tie
[1]School of Mechanical Engineering, Northeast Electric Power University, 132012, Jilin, China
[2]Zhejiang Zhoushan Cengang Wind Power Co., Ltd., 316053, Zhoushan, China

Abstract: The utilization efficiency of wind energy is directly affected by airfoil aerodynamic performance. So, it is important to study it. In this study, CFD software is used to analyze the aerodynamic performance of lift type vertical axis wind turbines at low Reynolds number. Three types of airfoil which are NACA2414, NACA4414 and NACA6414, are analyzed by numerical simulation, mainly study the influence of relative camber airfoil on wind turbine aerodynamic performance under different angle of attack and the change rule of airfoil aerodynamic parameters and the state of streaming for these three types of airfoil under different angle of attack is obtained. The result shows that the lift coefficient of airfoil under different Angle of attack and lift-drag ratio will increase, with relative camber airfoil increasing,the airfoil thickness keeping stable,but the airfoil drag coefficient has no obvious change, it will help the optimal design of airfoils for vertical axis wind turbines.

Key words: Vertical-axis wind turbine, blade airfoil, aerodynamic performance, relative camber

INTRODUCTION

The development of low wind speed of wind energy and utilization has profound significance of fossil to alleviating energy crisis and improve the natural environment (Lee *et al*., 2007). Inland areas in China mainly low wind speed area by the annual average wind speed primarily for 6-8 m sec^{-1} which has great development potential. Wind turbine is the medium of wind energy into electrical energy device; the impeller transforms wind energy into mechanical energy mean while mechanical energy is tranformed into electricity through the generator. Vertical axis wind turbines suitable for operation in low wind speed. Due to the blade aerodynamic performance of airfoil affects the impeller, the impeller structure of the fit and unfit quality directly affect the wind energy utilization of wind turbines (Jin, 2012; Zhang *et al*., 2009; Ji and Jorg, 2011; Timmer and Schaffarczyk, 2004; Liao *et al*., 2009). So, it's important content to choose the appropriate blade airfoil and optimize of the structure of the impeller for designing Vertical Axis Wind Turbine.

The NACA four digits aviation airfoil series is one types of the earliest low speed airfoils, compared with other early airfoil have higher maximum lift coefficient and low drag coefficient. Based on the CFD software and the two-dimensional unstructured grid for three different relative camber airfoil NACA2414, NACA4414, NACA6414 numerical simulation analysis of the aerodynamic performance to study of wind turbine work relative camber on airfoil aerodynamic performance of airfoil (Yang and Tong, 2011; Myose *et al*., 1996).

NUMERICAL RESEARCH METHODS

Using Fluent to numerical calculation, regardless of the pitch Angle of airfoil or parallel slide, so choose the steady-state nervier-stokes (RANS) equations as fluid control equation. Choose the standard model, the model is defined as:

$$\varepsilon = \frac{\mu}{\rho}\overline{\left(\frac{\partial u_i'}{\partial x_k}\right)\left(\frac{\partial u_i'}{\partial x_k}\right)} \quad (1)$$

So, the turbulent viscosity μ_t can be expressed as a function of k and e:

$$\mu_t = \rho C_\mu \frac{k^2}{\varepsilon} \quad (2)$$

Therefore, the standard transport equation is:

$$\frac{\partial(\rho k)}{\partial t} + \frac{\partial(\rho k u_i)}{\partial x_i} = \frac{\partial}{\partial x_j}\left[(\mu + \frac{\mu_t}{\sigma_k})\frac{\partial k}{\partial x_j}\right] + G_k + G_b - \rho\varepsilon - Y_M + S_k \quad (3)$$

$$\frac{\partial(\rho\varepsilon)}{\partial t} + \frac{\partial(\rho\varepsilon u_i)}{\partial x_i} = \frac{\partial}{\partial x_j}\left[(\mu + \frac{\mu_t}{\sigma_\varepsilon})\frac{\partial \varepsilon}{\partial x_j}\right] + C_{1\varepsilon}\frac{\varepsilon}{k}(G_k + C_{3\varepsilon}G_b) - C_{2\varepsilon}\rho\frac{\varepsilon^2}{k} + S_\varepsilon \quad (4)$$

Corresponding Author: School of Mechanical Engineering, Northeast Electric Power University, 132012, Jilin, China

$$\begin{cases} G_k = \mu_t(\frac{\partial u_i}{\partial x_j} + \frac{\partial u_j}{\partial x_i})\frac{\partial u_i}{\partial x_j} \\ G_b = \beta g_t \frac{\mu_t}{Pr_t}\frac{\partial T}{\partial x_i} \\ \beta = -\frac{1}{\rho}\frac{\partial \rho}{\partial T} \\ Y_M = 2\rho\varepsilon M_t^2 \\ M_t = \sqrt{k/a^2} \\ a = \sqrt{\gamma RT} \end{cases} \quad (5)$$

where, G_k is the average velocity gradient caused by turbulent kinetic energy; G_b Is said to cause a turbulent kinetic energy generated buoyancy effect; YM said compressible turbulent flow pulsation expansion for the total dissipation rate; For C_{1e}, C_{2e}, C_{3e}, the default value is C_{1e} = 1.44, C_{2e} = 1.92, C_{3e} = 0.09, σ_k, σ_e said the turbulent kinetic energy and turbulent dissipation prandtl of rate number and σ_k = 1.0, σ_e = 1.3; Prt for turbulent prandtl number, the default take Prt = 0.85; Gi said gravity acceleration on the direction of the i component; b according to the thermal expansion coefficient; M_t said turbulent Mach number; a for the sound velocity (Zhou *et al*., 2010; Han, 2009).

PHYSICAL MODEL AND BOUNDARY CONDITIONS

Geometric model set up: Involved in C type structured grid are generated by former processing software GAMBIT calculation of CFD, in order to meet the requirements of structured grid on the geometry calculation domain and for the convenient of grid generation, in addition to the wing type C boundary, the flow field of the wing leading edge and trailing edge of each set an extension to C boundary of auxiliary linear boundary, when calculated in accordance with the internal flow field processing, Fig. 1 shows the local grid around airfoils. In order to make the boundary conditions on the outer boundary is consistent with the surrounding environment, the length of the computational domain is 30 times the airfoil chord length and width is 20 times of the airfoil chord length, computational domain grid nodes, a total of 33251 grid cell count of 32880, because of the airfoil near wall flow field the parameter variation gradient is greater than the parameters of the far field gradient change, the airfoil near the encryption of the grid, the wing leading edge and trailing edge and airfoil type for key encryption area near the leading edge.

Convergence condition: for stationary flow calculations, with the increase of iteration steps, all airfoil aerodynamic performance parameter value smonitored (lift coefficient and drag coefficient, etc.) should be constant.

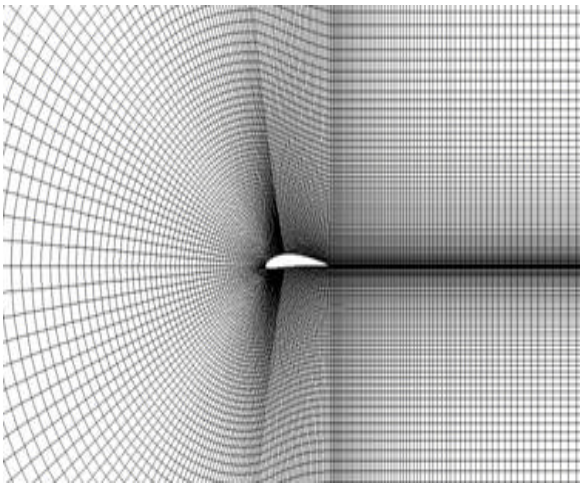

Fig. 1: Local grid around airfoil

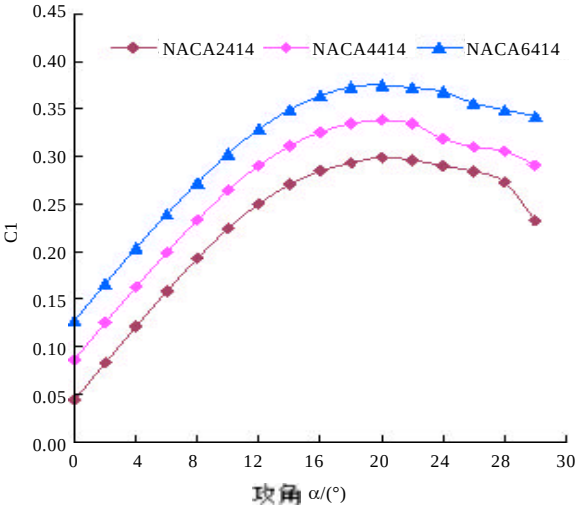

Fig. 2: Lift coefficient curves of 3 types of airfoils

Outside the Computational domain boundaries for the far field boundary conditions, the flow field is set to the entrance velocity inlet boundary conditions; the flow field is set to the pressure outlet boundary conditions for export. Given to flow rate, static pressure and temperature, etc., for the adiabatic wall slip conditions.Numerical simulation is implemented by changing the size of the Angle of attack where the flow angle varies from 0-30°.

The calculation results and analysis: Fig. 2 in 4 is with the Reynolds number Re = 1.6×10^5, NACA2414, NACA4414, NACA6414 different relative camber airfoils drag coefficient (Cd), lift coefficient (Cl) and lift-drag ratio (Cl/Cd) curves. As can be seen from the Fig. 2 and 3, when the Angle of attack is less than 16°, three airfoils of lift coefficient and drag coefficient are increased with the

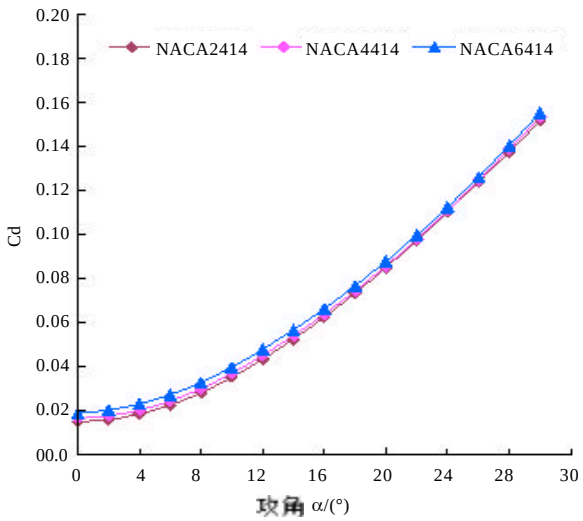

Fig. 3: Drag coefficient curves of 3 types of airfoils

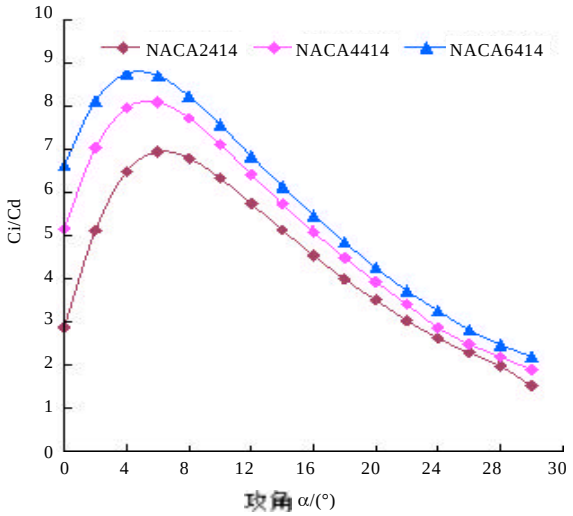

Fig. 4: Lift-drag ratio of 3 types of airfoils

increase of Angle of attack and rate is relatively stable, camber of airfoil lift significantly smaller than camber airfoil lift, but three airfoil drag coefficient are different; When the angle of attack around in 21°, three types of airfoils maximum lift coefficient are achieved, along with the increase of Angle of attack, three types of lift coefficient of airfoil are began to decline and the decreasing amplitude of uncertain. The drag coefficient is rising sharply. This is mainly due to the air in appeared on the surface of the airfoil flow separation, separation and increases with the increase of Angle of attack, Separation area leads to large form eddy current, lose airfoil flow effect.

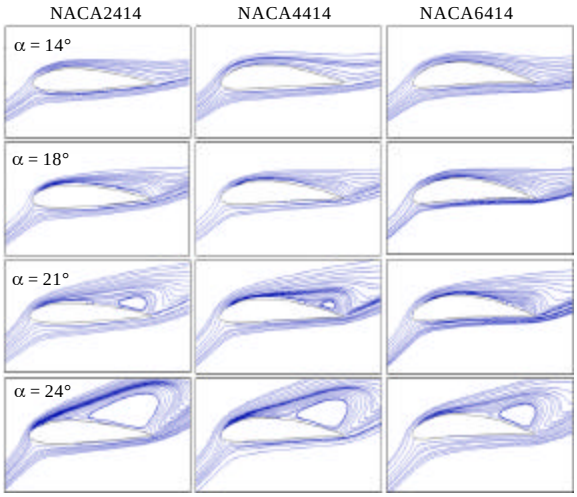

Fig. 5: Type three wing Angle of attack of 14, 18, 21 and 24° around the flow chart

Table 1: Maximum and average lift-drag ratio table of three airfoils when α between 0 and 12°

	NACA2414	NACA4414	NACA6414
(Cl/Cd) max	6.95 (α = 6°)	8.10 (α = 6°)	8.76 (α = 4°)
(Cl/Cd) avg	5.76	7.08	7.84

As shown in Fig. 4, three types of airfoils maximum lift-drag ratio are all appeared in the scope of the small Angle of attack, the big camber airfoil lift-drag ratio is greater than the small. With the increase of the airfoil camber airfoil lift-drag ratio amplitude decreases. From the Table 1,the maximum and the average of three types of airfoils NACA6414 airfoils of angle of attack between 0 and 12° are most closely, therefore, the design Angle of attack between 0 and 12° low Reynolds number in the range of the impeller blade airfoil NACA6414 is suitable for using, so it can ensure wind turbine have big wind energy use efficiency.

Figure 5 is three different camber of airfoils in angle of attack of 14, 18, 21 and 24° around the flow chart. From the Fig. 5, with the increase of Angle of attack, the airfoil surface boundary layer gradually separate, when the angle of attack is more than 21° (maximum lift coefficient) largest trailing edge lead edge backflow phenomenon is more intensed than the angle of attack is less than 21°. So, when angle of attack is more than 21°, with the increase of Angle of attack, dynamic stall airfoil phenomenon began to appear. Small camber airfoil appeared earlier than large camber airfoil tail vortex, the smaller the camber, the earlier tail vortex appears and separation point is close to the front.

SUMMARY

- When the airfoil thickness of relative phase is same, in a certain range, increasing the relative camber airfoil can improve the lift coefficient of airfoil and lift-drag ratio
- Under the condition of low Reynolds number and small angle of attack, with the change of the angle of attack, relatively large camber airfoil lift-drag ratio changes smoothly which can maintain at a high level
- Small camber airfoil dynamic stall occurs earlier than large camber airfoil, the smaller the camber, the earlier tail vortex appears and separation point is close to the front
- Aalysis of three different relative camber airfoil, NACA6414 is suitable for low Reynolds number airfoil and small Angle of attack range of the rotation of the impeller blade shape design, so the wind turbine can abtain relatively large wind energy utilization

REFERENCES

Han, Z.Z., 2009. The FLUENT Software-Fluid Simulation Calculation of Engineering Examples and Analysis. Beijing University of Science and Technology Press, Beijing, China, ISBN: 978-7-5640-2604-2.

Lee, Z.C., R. Zhu, X.F. He and D. Zhang, 2007. Wind energy resource assessment methods research. Acta Meteorol. Sin., 65: 708-717.

Liao, M.F., R. Gasch and J. Twele, 2009. Wind Power Generation Technology. 1st Edn., Northwestern Polytechnical University Press, China, ISBN: 978-7-5612-2538-7.

Jin, K., 2012. Computation and analyses on the aerodynamic performance of the special airfoils for wind turbine. Lanzhou University of Technology.

Ji, X.N. and S. Jorg, 2011. Design and analysis of small-scale vertical axis wind turbine. Proceedings of the IET Conference on Renewable Power Generation, September 6-8, 2001, Edinburgh, UK., pp: 1-10.

Myose, R., I. Heron and M. Papadakis, 1996. Effect of gurney flaps on a NACA 0011 airfoil. AIAA Paper 96-0059.

Timmer, W.A. and A.P. Schaffarczyk, 2004. The effect of roughness at high Reynolds numbers on the performance of aerofoil DU 97-W-300Mod. Wind Eng., 7: 295-307.

Yang, C.X. and G. Tong, 2011. Numerical computation and analyses on the blade aerodynamic performance of a horizontal axis wind turbine rotor. Proceedings of the Asia-Pacific Power and Energy Engineering Conference, March 25-28, 2011, Wuhan, China, pp: 1-4.

Zhou, J.J., G.Q. Xu and H.J. Zhang, 2010. FLUENT Software Engineering Technology and Instance Analysis. 1st Edn., China Water Conservancy and Hydropower Press, China, ISBN: 978-7-5084-7491-5.

Zhang, J.L., Z.G. Zhou and Y.S. Lei, 2009. Design and research of high-performance low-speed wind turbine blades. Proceedings of the World Non-Grid-Connected Wind Power and Energy Conference, September 24-26, 2009, Nanjing, China, pp: 1-5.